Bioorganic Chemistry 151 (2024) 107663

Contents lists available at ScienceDirect

Bioorganic Chemistry

journal homepage: www.elsevier.com/locate/bioorg

Intersite communication in dimeric enzymes highlighted by structural and thermodynamic analysis of didansyltyrosine binding to thymidylate synthases

Alberto Venturelli [a], Giambattista Guaitoli [a,b], Davide Vanossi [c], Francesca Saitta [d], Dimitrios Fessas [d], Simone Vitiello [a], Giulia Malpezzi [a,e], Daniele Aiello [a], Stefania Ferrari [a], Donatella Tondi [a], Glauco Ponterini [a,*], Maria Paola Costi [a,*]

[a] Dipartimento di Scienze della Vita, University of Modena and Reggio Emilia, Via Campi 103, 41125 Modena, Italy
[b] Evotec SE, Biophysic - Essener Bogen 7, 22419 Hamburg, Germany
[c] Dipartimento di Scienze Chimiche e Geologiche, University of Modena and Reggio Emilia, Via Campi 103, 41125 Modena, Italy
[d] Dipartimento di Scienze per gli Alimenti, la Nutrizione e l'Ambiente, DeFENS, Università degli Studi di Milano, Via Celoria 2, 20133 Milano, Italy
[e] Clinical and Experimental Medicine (CEM) PhD Program, University of Modena and Reggio Emilia, Via G. Campi 287, 41125 Modena, Italy

ARTICLE INFO

Keywords:
Thymidylate synthase
Dimeric protein
Subunit anti-cooperativity
Fluorometric titration
Isothermal titration calorimetry

ABSTRACT

Intersite communication in dimeric enzymes, triggered by ligand binding, represents both a challenge and an opportunity in enzyme inhibition strategy. Though often understestimated, it can impact on the *in vivo* biological mechansim of an inhibitor and on its pharmacokinetics. Thymidylate synthase (TS) is a homodimeric enzyme present in almost all living organisms that plays a crucial role in DNA synthesis and cell replication. While its inhibition is a valid strategy in the therapy of several human cancers, designing specific inhibitors of bacterial TSs poses a challenge to the development of new anti-infective agents. N,O-didansyl-L-tyrosine (DDT) inhibits both *Escherichia coli* TS (*Ec*TS) and *Lactobacillus casei* TS (*Lc*TS). The available X-ray structure of the DDT:dUMP:*Ec*TS ternary complex indicated an unexpected binding mode for DDT to EcTS, involving a rearrangement of the protein and addressing the matter of communication between the two active sites of an enzyme dimer. Combining molecular-level information on DDT binding to *Ec*TS and *Lc*TS extracted from structural and FRET-based fluorometric evidence with a thermodynamic characterization of these events obtained by fluorometric and calorimetric titrations, this study unveiled a negative cooperativity between the DDT bindings to the two monomers of each enzyme dimer. This result, complemented by the species-specific thermodynamic signatures of the binding events, implied that communication across the protein dimer was triggered by the first DDT binding. These findings could challenge the conventional understanding of TS inhibition and open the way for the development of novel TS inhibitors with a different mechanism of action and enhanced efficacy and specificity.

1. Introduction

Thymidylate synthase (TS) is a ubiquitous enzyme involved in the synthesis of deoxythymidine monophosphate (dTMP) from deoxyuridine monophosphate (dUMP). The inhibition of TS results in a deficiency in the intracellular concentration of dTMP, causing DNA synthesis alteration and provoking DNA damage and cell death [1]. The TS enzyme is present in all living organisms. In some microorganisms such as *Mycobacterium Tuberculosis* a different protein, namely flavin-dependent thymidylate synthase (ThyX), contributes to the dUMP synthesis [2]. In humans, TS (hTS) is a validated clinical target in anticancer therapy [1] and anti-TS drugs such as 5-fluorouracil (5FU) (metabolized intracellularly in 5-fluorodeoxyuridine monophosphate, FdUMP) and antifolates, i.e., compounds structurally similar to the folate cofactor, such as pemetrexed and raltitrexed (Fig. 1) are currently in use. On the other hand, antibacterial drugs targeting TSs, although potentially interesting, are not available partly because of the structural and functional similarities between the bacterial and human enzymes. Some attempts have been performed to identify specific compounds against *Escherichia coli* TS (*Ec*TS) and a few leads were discovered such

* Corresponding authors at: Department of Life Science, University of Modena and Reggio Emilia, Modena, Italy.
E-mail addresses: glauco.ponterini@unimore.it (G. Ponterini), mariapaola.costi@unimore.it (M. Paola Costi).

https://doi.org/10.1016/j.bioorg.2024.107663
Received 1 June 2024; Received in revised form 17 July 2024; Accepted 18 July 2024
Available online 20 July 2024
0045-2068/© 2024 The Author(s). Published by Elsevier Inc. This is an open access article under the CC BY license (http://creativecommons.org/licenses/by/4.0/).

as phenolphthalein, PTH [3], a few naphtalein, α156 [4], and phtalimidic [5] derivatives, N,O-didansyl-L-tyrosine (DDT) and derivatives [6–8] (Fig. 1). Because of its important clinical relevance, the structures and catalytic mechanisms of the TS proteins have been widely studied. According to the 6–9-step catalytic mechanism of bacterial TS, the enzyme catalyzes the reductive methylation of dUMP using 5-mehylene-tetrahydrofolate cofactor (mTHF) as the carbon unit donor and reducing agent [9]. TS enzymes are multi-subunit proteins and the two active sites in the dimeric protein are exposed to the surface and separated by approximately 30–36 Å. The mechanism of action, with the resulting amounts and time of delivery of the end products are influenced by the crosstalk among the protein subunits [10].

Attempts have been done to understand the intersubunit communication upon ligand binding in such flexible proteins as TSs and its possible role/consequences. For example, in *Ec*TS and *Lc*TS, whose active sites are exposed to the protein surface and are separated from the inter-monomer interface [11], binding of the dUMP substrate does not seem to cause relevant structural changes, while the subsequent binding of the cofactor (mTHF) to the dUMP-*Ec*TS binary complex causes the C-terminus of the protein to move 5 Å toward the active site. Also, the two catalytic sites, one per monomer, do not act simultaneously and there is evidence for a negative regulation of one site while the other exerts its catalytic action upon interaction with the substrates. This is defined as 'half-the-sites reactivity' and, being the two sites approximately 35 Å apart, it suggests the occurrence of long-range conformational rearrangements of the protein related with substrate/cofactor binding and the subsequent catalytic function [12,13].

In order to deduce a communication/cooperativity between the intersubunits, a marked and functionally significant structural change should be observed and the corresponding changes in the associated thermodynamic functions measured. In this regard, a literature survey highlights some ambiguities. Some authors reported that NMR and ITC experiments conducted on bacterial *Ec*TS had indicated no cooperativity between the two binding events, one per active site, of both the substrate and the cofactor [14]. On the other hand, other NMR experiments showed a positive cooperativity for dUMP binding to human TS [15]. Little or no information has been provided by these techniques about communication between the protein monomers in cases of binding of non-cofactor-analogue inhibitors [16]. X-ray crystallography was of little help in the investigation of substrate binding cooperativity. In fact, out of the more than 231 X-ray structures available in the PDB, (PDB May2024), among TS:substrate or TS:substrate-analog complexes only that of *Lc*TS (1LCA) shows an asymmetric dimer with two dUMP molecules and only one molecule of a cofactor-analogue bound. In this case the communication between the monomers is evident and supports the half-the-sites reactivity [16,17]. The communication between the two active sites of the TS enzymes likely depends on the ligand chemical nature. Calorimetric and spectroscopic techniques can provide information on the thermodynamics of the interaction of TS with ligands different from the substrates, e.g., TS inhibitors, that can shed light on the interplay between the two monomers. A number of X-ray crystal structures of the protein:inhibitor complexes showed that non-substrate analogs can bind within the protein active site [18]. Among them, N,O-didansyl-L-tyrosine (DDT), inhibiting both *Ec*TS and *Lc*TS, is the inhibitor with the highest steric hindrance [6,7] (Fig. 1). DDT showed similar inhibition constants (K_i) against *Ec*TS and *Lc*TS, 1.4 and 1.8 μM, and 30–40 times lower activity against *human* TS (K_i^{hTS}/K_i^{TS}) [6,7]. The available X-ray crystal structure of the *Ec*TS:DDT:dUMP ternary complex

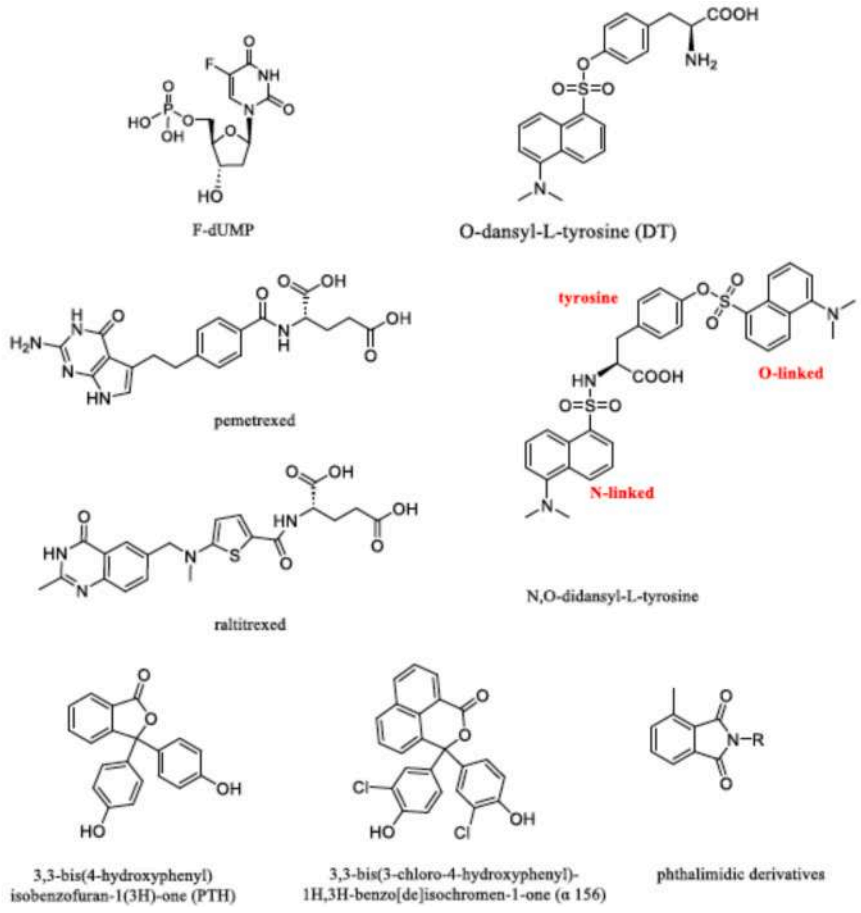

Fig. 1. Chemical structures of human (pemetrexed, raltitrexed) and bacterial TS inhibitors, O-dansyl –L-tyrosine, DT, N,O-didansyl-L-tyrosine (DDT), phenolphthalein (PTH), and naphtalein derivatives (α156) and phtalimidic derivatives.

(PDB 1JG0) shows that the bulky DDT molecule occupies both active sites taking a folded conformation with the *N*-linked dansyl establishing a stacking interaction with the tyrosine moiety following a large protein re-organization [7]. On the other hand, in the *Lc*TS:DDT model described in a previous study [6,7] the same compound preferably binds both active sites in an extended conformation in which no stacking interactions can be observed. The conformational selection promoted by *Ec*TS and *Lc*TS in the DDT binding might be a result of a smaller active site in *Ec*TS with respect to *Lc*TS. However, the difference in the active site microenvironment such as crucial aminoacid changes could concurrently affect the conformational preference. A structural analysis of the active sites of the enzymes can clarify this aspect.

The described peculiarities of the DDT binding to *Ec*TS/*Lc*TS provide an opportunity to deepen our knowledge of intersite communication in TS proteins triggered by ligand binding. This is the main aim of the present work. This study might reveal differential responses among bacterial TS species and provide a new driving concept in the design of specific TS inhibitors. To this aim we have investigated DDT binding to *Ec*TS and *Lc*TS by means of fluorescence spectroscopy and isothermal titration calorimetry (ITC). The results have revealed differences in the thermodynamic profiles of DDT binding to the two proteins. Such differences led us to make reasonable considerations about associated different modulations of the intersite communication that result in a negative cooperativity between DDT binding to the two enzyme monomers. New mode of inhibition can be achieved through the fine tuning of the ligand binding mode to the homodimeric enzymes and it is

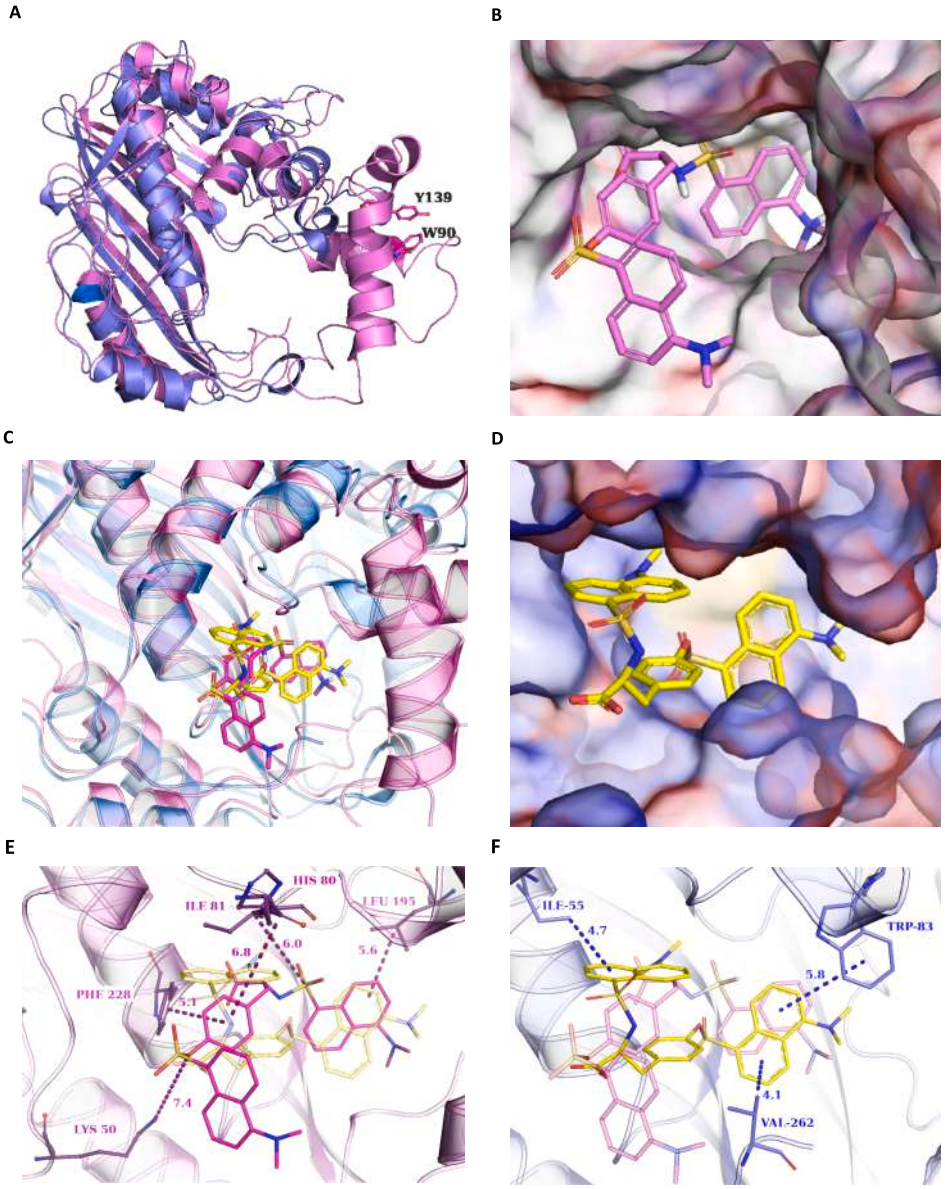

Fig. 2. A. Overlap of X-ray strucures of *Ec*TS (PDB 1JG0, blue) and *Lc*TS (PDB 1LCA, magenta) obtained using the align function of PyMOL (Molecular Graphics System, version 2.5.2). The small domain is reported in magenta color (aa 90–139). MatchAlign: score 807.500. Align: 265 atoms aligned. RMSD=0.836 (236 to 236 atoms). B. Detailed view of the *Lc*TS:DDT:dUMP model. DDT is in the extendend conformation. C. Alignment of *Ec*TS (PDB 1JG0, blue) with DDT (yellow), *Lc*TS pink with DDT hotpink derived from the computational study. D. DDT pose in the active site in the X-ray crystal structure of *Ec*Ts (PDB 1JG0) where the distal *N*-dansyl establishes a stacking interaction with the tyrosine ring. E. Binding pose of DDT in the *Lc*TS protein (PDB 1LCA), showing interactions with Lys50, Phe228, Ile81, His80, and Leu195 (residues indicated in purple). The extended conformation observed in *Lc*TS is shown in light pink. F. X-ray structure of *Ec*TS (PDB 1JG0) with DDT, showing the van der Waals interactions with Ile55, Trp83, and Val62. The folded conformation of DDT found with *Ec*TS is shown in light yellow. The snapshot images were generated with PyMOL. (For interpretation of the references to color in this figure legend, the reader is referred to the web version of this article.)

possible to translate the concept of altering the intersites communication to other dimeric enzymes.

2. Results

2.1. EcTS and LcTS structural analysis

Comparisons by alignment of TSs of several pathogenic organisms using BLAST (NCBI) showed that *Ec*TS (1KZI PDB) shares high homology with the other pathogenic TSs, including *Pseudomonas aeruginosa* (UniProt sequence B7V2Q5), 69.7%, *Neisseria meningitidis* (UniProt sequence A1KVB3), 71.21 %, *Shigella flexneri* (UniProt sequence P48464), 99.62 %, *Neisseria gonorrhoeae* (UniProt sequence A0A378VTM3), 76.80 %, *Mycobacterium tuberculosis* (PDB 3QJ7, ThyA), 66.29 %, *Lactobacillus casei* (PDB 1LCA), 51.13 %, *Staphylococcus aureus* (PDB 4DQ1), 51.13 % and human (6QXG PDB), 51.06 % (Supplementary Material, Fig. 1.1). The same applies to *Lc*TS which, although not belonging to a pathogenic bacterium, shows some similarity with pathogenic species such as *Staphylococcus aureus*, *Bacillus Antracis* and *Neisseria gonorrhoeae* (Supplementary Material, Fig. 1.1).

The residues forming the active sites of *Lc*TS and *Ec*TS are highly conserved and superimposition of the X-ray crystal structures of the apoenzymes shows a very low RMSD (0.836). On the other hand, the 50 amino acids of the active site portion of *Lc*TS defined as the 'small domain' (residues 90 to 139 in *Lc*TS), are not present in *Ec*TS and *h*TS. The lack of this domain makes the active site of *Ec*TS smaller than that of *Lc*TS (Fig. 2A, B). However, while the total amino acid similarity between *Lc*TS and *Ec*TS is only 51.13 %, the folate-cofactor binding domain in the active site is highly conserved with an amino acid similarity over 70 %. Hence, inhibitors structurally related to the folate cofactor can hardly discriminate between different TS species.

On the other hand, one may expect that those TS inhibitors that are not structurally related to the substrates, by binding to portions of the active site different from the areas responsible for substrate recognition, can discriminate among TS species and behave as specific allosteric inhibitors [16,18]. Because the *Ec*TS active site is significantly smaller than the *Lc*TS active site, such a large molecule as DDT might be expected to bind to *Ec*TS with a lower affinity than *Lc*TS. Instead, DDT showed a similar affinity for the two enzymes [16]. In the X-ray *Ec*TS:DDT:dUMP ternary complex structure (Fig. 2C, D, F) two DDT molecules are bound to *Ec*TS, one to each of the two identical monomers, and the hydrogen bonding and van der Waals interactions between DDT, dUMP and the protein are the same at both binding sites [19,20]. The O-linked dansyl ring of DDT sits in the binding domain of the quinazoline ring of the folate cofactor but the ligand takes a rather unique compact conformation, with the *N*-linked dansyl ring folded and stacked over the tyrosine phenyl ring of the ligand, a conformation not predicted by molecular dynamic studies [7]. DDT binding is developed with an extensive rearrangement of the residues of the active site, with a displacement of the alpha carbons up to 6 Å relative to other ternary complexes. The van der Waals contacts of DDT with Ile 55, Trp 83 and Val 262 found in the structure of *Ec*TS can be maintained in *Lc*TS where such residues are conserved (Fig. 2E and F), but not in *h*TS. This crucial difference may be responsible for the lower affinity of DDT towards the human enzyme and its species specificity. All attempts to obtain the X-ray crystal structure of the ternary complex *Lc*TS:DDT:dUMP failed. Molecular dynamics simulations of *Lc*TS:DDT:dUMP have suggested that DDT could adopt two binding conformations: a folded conformation in which the *N*-dansyl forms a stacking interaction with the tyrosine moiety and a semi-folded (or extended) conformation, the latter being preferred [19,20]. These results led us to propose that the folded conformation of DDT be preferred by *Ec*TS while the semi-folded conformation by *Lc*TS (Fig. 2).

The computational studies previously performed to generate an *Ec*TS:DDT:dUMP model have been repeated in the present study to confirm the results previously obtained (Supplementary Material 2.1).

2.2. Fluorometric determination of the DDT/Ec(Lc)TS binding affinities and molecular probing

The DDT/*Ec*(*Lc*)TS binding was investigated fluorometrically. To gain control on the nature of the tryptophan (W) fluorescence quenching that we observed upon addition of DDT to the proteins, we decided to estimate the Forster's distance (R_0) for the W/DDT excitation-energy donor–acceptor pair, i.e., the distance at which the W-to-DDT excitation energy transfer efficiency is 0.5. This characteristic distance was then compared with the W/DDT distances in the X-ray crystal structure of the *Ec*TS:DDT:dUMP complex. According to the *Ec*TS and *Lc*TS structures, some conformational differences involve the W residues upon DDT binding when compared to the apo form of the enzymes (Fig. 4A, B). Out of the fourteen W in the *Ec*TS and *Lc*TS dimers, twelve (W61, W80, W83, W98, W101, W133, W61′, W80′, W83′, W98′, W101′ and W133′ (based on the *Ec*TS numbering) are conserved and form a line that stretches across both monomers (Figs. 3 and 4).

In the crystal structure of the *Ec*TS:DDT:dUMP complex, DDT lies 8 and 6 Å from W80 and W83, 13–14 Å from W61 and W201, 15–17 Å from W98 and W133, and 22 Å from W101 (Fig. 4A, B, C, D); also, it lies 27–28 Å from two W of the opposite monomer (W101′, W133′) and 29 Å from W201′ and W98′ (Fig. 4E, F).

To investigate the distance dependence of the efficiency of W-to-DDT energy transfer, we designed a chemical model that could enable us to measure the relative change in fluorescence emission intensity of W (I_f), hence the relative quenching efficiencies, with increasing distance from DDT (Fig. 5A). The chemical model was designed in order to have on one side the W, the energy donor, linked to dansyl tyrosine (DT, the acceptor) on the other side, through a polyproline spacer $(P)_n$ of variable lengths: W-$(P)_n$-DT (n = 3,6,9,12, Fig. 5B, C). The polyproline linkers represent relatively rigid spacers that establish known distances between the energy transfer partners [21]. The fluorescence emission spectra of isoabsorbing, freshly prepared samples of these compounds in a 9:1 (v/v) water–ethanol mixture are shown in Fig. 5. The corresponding quenching efficiencies were determined in water–acetone 9:1 and in dichloromethane (DCM) as $Q\% = 1 - I_f(W\text{-}(P)_n\text{-}DT)/I_f(W\text{-}(P)_3)$ and are reported in Table 1.

The quenching efficiency drops regularly with increasing number of proline units in water–ethanol 9:1, thus suggesting that the $(P)_n$ spacer assumes in this aqueous environment a relatively rigid geometry that is maintained in the four compounds with n = 3, 6, 9 and 12. A critical discussion of this point is given in [21]. To test the effect of the added

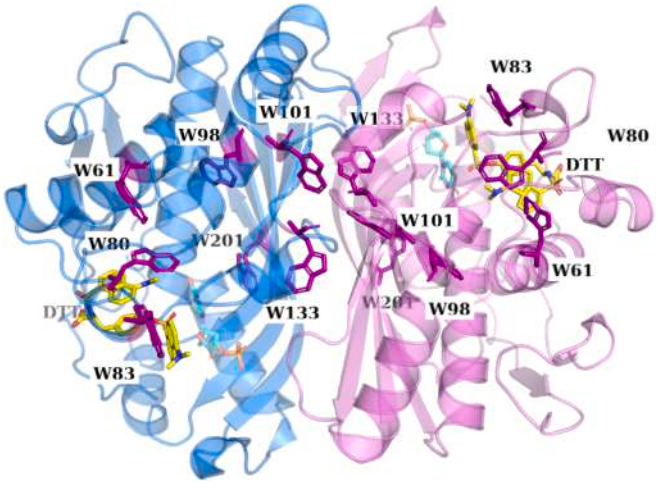

Fig. 3. X-ray structure of the ternary complex *Ec*TS:DDT:dUMP. The DDT ligand is reported in yellow, dUMP is reported in cyan; monomer A is reported in blue with tryptophans in purple, monomer B in violet wtih tryptophans in purple. (For interpretation of the references to color in this figure legend, the reader is referred to the web version of this article.)

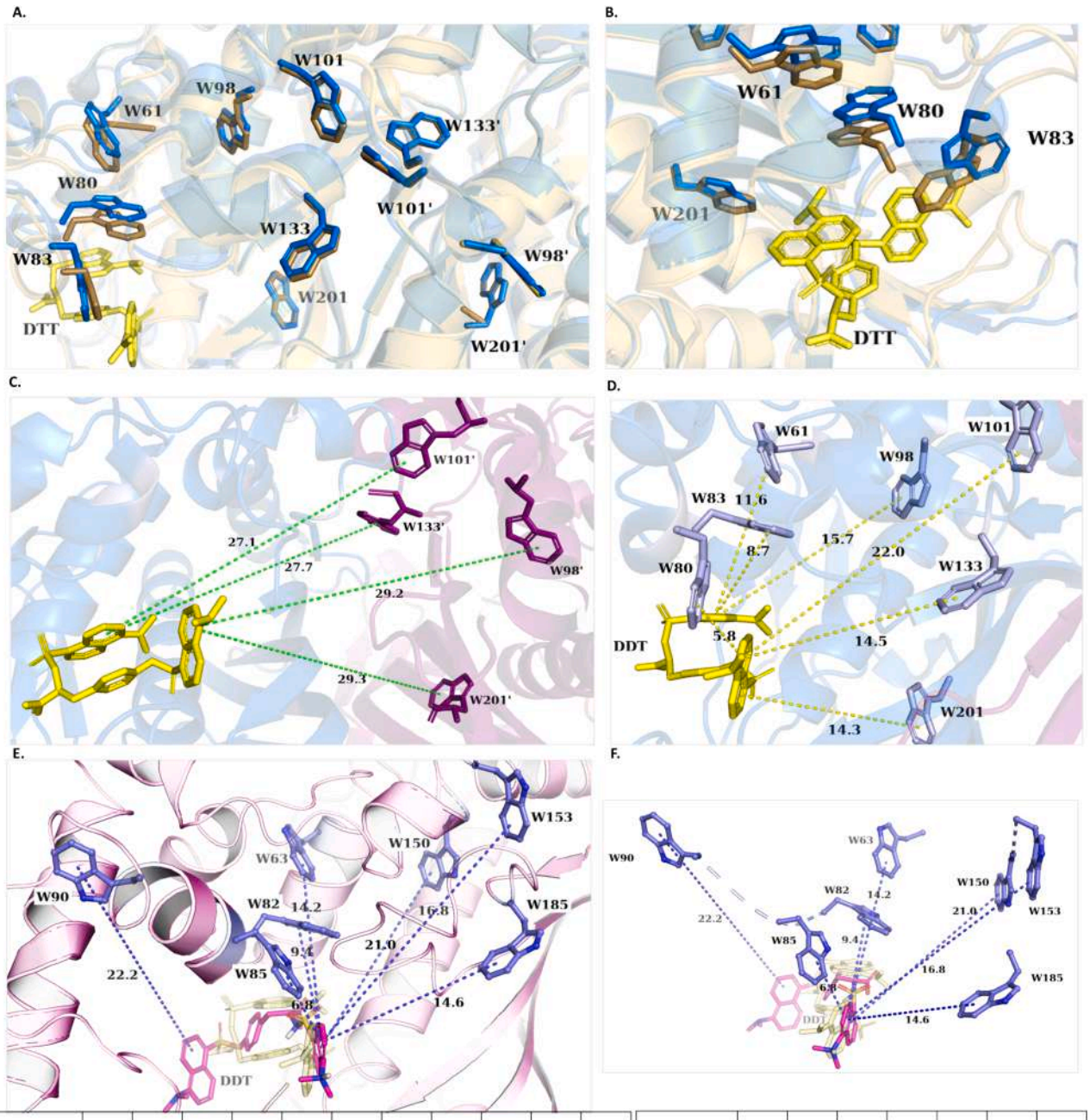

EcTs (TRP)	W80	W83	W61	W201	W98	W133	W101	W133'	W101'	W201'	W98'
DISTANCE DTT (Å) (Pymol software)	8.2	5.8	13.0	14.3	17.1	14.5	22.0	27.7	27.1	29.3	29.2
legend	Yellow distance Monomer 1							Green distance Monomer 2			

LcTS (TRP)	W82	W85	W90	W185	W63	W150	W153
DISTANCE DTT (Å) (Pymol software)	9.4	6.8	22.2	14.6	17.1	21	16.8
legend	Blue distance Monomer 1						

Fig. 4. W-DDT distances in the *Ec*TS:DDT:dUMP X-ray crystal structure and in the *Lc*TS:DDT:dUMP model. A. Alignment of the *Ec*TS (PDB 1KZI, blue) with the *Ec*TS: DDT:dUMP (PDB 1JG0, yellow) structures. B. Same picture as A with W83 and W80 represented in detail (RMSD 0.616 Pymol) C. Distances (green dashed lines) between the DDT molecule bound to one *Ec*TS monomer (blue) and the indoles of the four tryptophans of the same monomer (pink). D. Distances (yellow dashed lines) between DDT bound to one *Ec*TS monomer (blue) and the indoles of the seven tryptophans of the same monomer (blue). E. Distances (blue dashed lines) between DDT (hotpink) bound to one *Lc*TS monomer (pink) and the indoles of the seven tryptophans of the same monomer (blue). In yellow with 90% of transparency, the conformation of DTT found in the *Ec*TS:DTT:dUMP ternary complex. F. Details of the distances, same as in E, without the cartoon structure of the *Lc*TS binding model of compound DDT in the active site. All distances are given in Å and are reported, together with the color correspondence, at the bottom. (For interpretation of the references to color in this figure legend, the reader is referred to the web version of this article.)

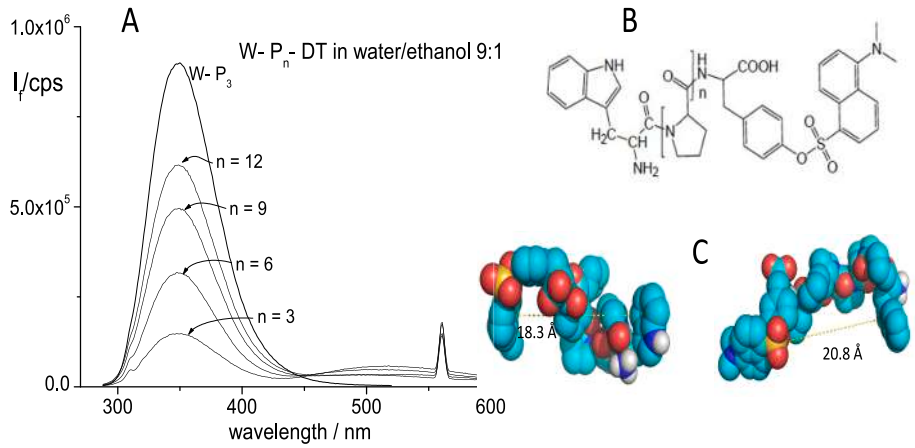

Fig. 5. A. Emission spectra of W-(P)$_n$-DTy in 9:1 (v/v) water/ethanol, wavelength 350 nm. Excitation wavelength: 280 nm. Intensities are given in counts per second (cps). B. Chemical structure of the W-(P)$_n$-DTy used as models to investigate the dependence of the observed efficiency of W-DTy excitation-energy transfer on the W-to-dansyl distance. C. 3D model of the W-(P)$_6$-DTy compound. Two preferred conformations, resembling a type II helix according to the angular parameters derived from the crystal structure, are represented with the corresponding W-dansyl distances.

Table 1
Quenching efficiencies (*Q%*) of W-(P)$_n$-DTy in 9:1 water–ethanol and in dichloromethane (DCM). *Q%* = 1- I$_f$(W-(P)$_n$-DT)/I$_f$(W-(P)$_3$), where I$_f$ is the intensity at the emission maximum, 348 nm in the water–ethanol mixture and 323 nm in DCM.

Compound	*Q*% in WA 9:1	*Q*% in DCM
W-(P)$_3$-DTy	81	−3
W-(P)$_6$-DTy	57	39
W-(P)$_9$-DTy	36	31
W-(P)$_{12}$-DTy	24	10

terminal W and DTy on the polyproline conformation we performed a conformational study on the W-(P)$_6$-DTy compound (see the Materials and Methods for details). Attachment of W and DTy at, respectively, prolines 1 and 6, did not alter the peptide conformational preference, i.e., a type II helix (Fig. 5C), previously identified for polyproline linkers [21]. The two preferred conformations of W-(P)$_6$-DT corresponded to W-DT distances of 18.3 and 20.8 Å (Fig. 5C). The data in dichloromethane indicate a more complex dependence of the quenching efficiency on the number n of P units and suggest that water as a solvent is necessary to obtain a relatively linear geometry of the P$_n$ spacer. According to the data in 9:1 water–ethanol, for the W-DTy donor–acceptor pair the characteristic Förster distance, i.e., the distance at which the quenching efficiency is 50 % (r$_0$), is that corresponding to n = 6–7, i.e., according to the above conformational model for the *hexa*-prolyne peptide, nearly 20 Å.

Based on the distances between the DDT molecule and the W units given above for the *Ec*(*Lc*)TS/DDT complexes (Fig. 4), this value supports the concept that each DDT molecule may quench the emission of W80, W83, W61 and W201, with an efficiency larger than 50 %, W98, W133 and W201 with an efficiency around 50 % and with lower, but non-negligible efficiencies several W of the other *Ec*TS monomer. Consistently with this expectation, the overall triptophan fluorescence of the two bacterial TSs (*Lc*TS, $\lambda_{max}^{fluo} = 339$ nm, and *Ec*TS, $\lambda_{max}^{fluo} = 337$ nm) was markedly quenched upon addition of DDT to dUMP-saturated *Ec*(*Lc*) TS (Fig. 6). Radiative energy transfer between these compounds was negligible since most of the signal quenching occurred with absorbances of DDT in the spectral emission range of W lower than 0.05 over 1 cm path length. Hence, the observed quenching is attributed to radiationless excitation energy transfer and represents direct evidence of DDT binding to the proteins in solution.

We analyzed the overall emission intensity of the Ws of *Ec*TS and of *Lc*TS *vs*. DDT concentration in terms of sequential binding of two DDT molecules (L) per TS dimer (P) with different affinities: $P + L \rightleftharpoons PL$, $PL + L \rightleftharpoons PL_2$, P indicating the protein and L the DDT ligand. The system of four equations in the four unknown concentrations [P], [L], [PL], [PL$_2$],

$$K_1 = \frac{[PL]}{[P][L]}, K_2 = \frac{[PL_2]}{[PL][L]}, [P]_{Tot} = [P] + [PL] + [PL_2], [L]_{Tot} = [L] + [PL] + 2[PL_2] \quad (4)$$

was solved for chosen values of K$_1$ and K$_2$ and for the current values of [L]$_{Tot}$ and [P]$_{Tot}$ (the latter being constant for a given titration apart from small corrections for dilution effects). The fractional decrease in W emission intensity, $\Delta F = (F_0\text{-}F([P]_{Tot} = \text{const}, [L]_{Tot}))/F_0$, where F$_0$ is the fluorescence intensity in the absence of ligand, was expressed in terms of quenching contributions from protein molecules bound to one or two DDT molecules according to

$$\Delta F = \Delta f_1 \cdot \nu_1 + \frac{\Delta f_2}{2} \cdot \nu_2, \quad (5)$$

where $\Delta f_{1,2}$ are the fractional changes in the macromolecule fluorescence due to attachment of one or two ligands and ν_i is the number of moles of ligand bound in the i-th binding state (1 or 2 per macromolecule) divided by the total number of moles of macromolecule, i.e., $\nu_1 = [PL]/[P]_{Tot}$, $\nu_2 = 2[PL_2]/[P]_{Tot}$ [22]. As described below and in the Supplementary Material, the Δf_i/i values proved different from each other, namely, $\Delta f_1 > \Delta f_2/2$, and this finding prevented us from analyzing the $\Delta F/L_T$ data according to the standard Scatchard approach. Instead, ΔF at the current, constant [P]$_{Tot}$ and at increasing values of [L]$_{Tot}$ was computed according to eq. (5) with a chosen value of Δf_1, with the $\nu_{1,2}$ obtained from solution of eqs. 1–4 with assumed values of K$_{1,2}$, and taking Δf_2 as the asymptotic limit of ΔF for [L]$_{Tot}$→ ∞. Calculated and experimental values of ΔF as functions of [L]$_{Tot}$ were plotted and compared; the fitting parameters, K$_1$, K$_2$, Δf_1 and Δf_2, were iteratively adjusted to reach a satisfactory agreement, judged on the basis of variance. Examples of fitting to experimental data sets are shown in Fig. 6. With both enzymes, the best-fit values of Δf_1 were 0.70 ± 0.05; those of Δf_2 were 0.85 ± 0.05 for *Ec*TS and 0.90 ± 0.05 for *Lc*TS. Uncomplete W emission quenching by DDT in the TS-DDT complexes is consistent with the r$_0$ and the r$_{W\text{-}DDT}$ distances given above. When the conditions for the Förster mechanism to be the dominant mechanism of W-to-DDT excitation-energy transfer within the protein-DDT complexes are fulfilled, i.e., typically for a distance between a donor and an acceptor (r$_{DA}$) larger than 1 nm, the efficiency of quenching, ϕ_Q, is expressed as $r_0^6/(r_0^6 + r_{DA}^6)$ and quenching is complete (say, $\phi_Q \geq 95$ %) only if at least one DDT molecule lies within a distance 0.6 r$_0$ from each

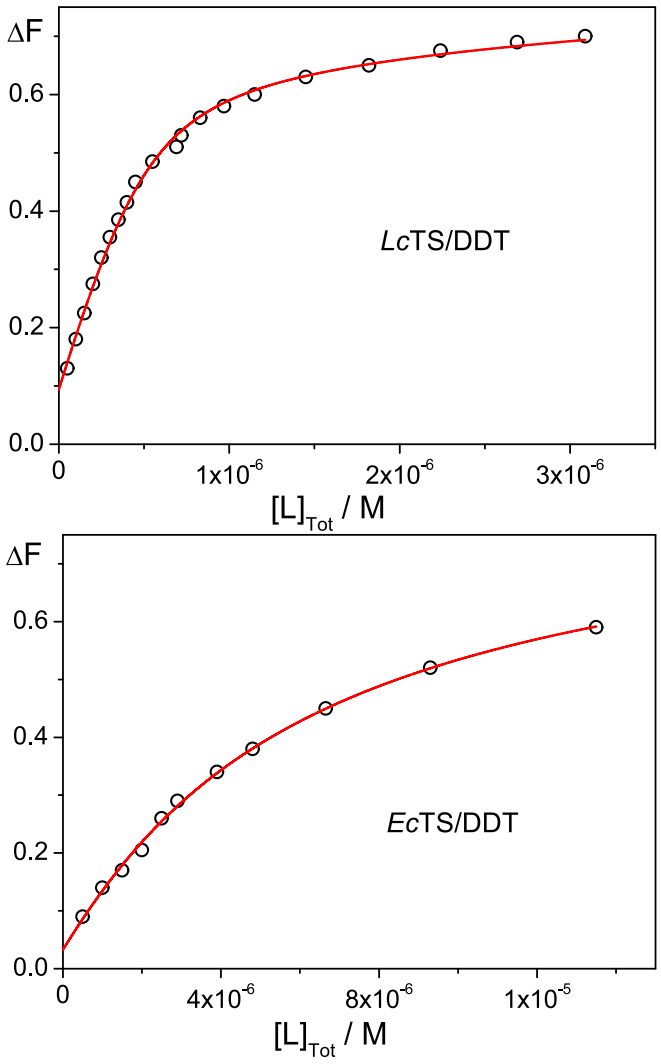

Fig. 6. Fractional decrease ($\Delta F=(F_0-F)/F_0$, see text) of *Ec*TS and *Lc*TS W fluorescence at 337 and 339 nm, respectively, upon addition of DDT (L). Initial protein concentrations ($[P]_{Tot}$): $1 \cdot 10^{-6}$ M (*Ec*TS), $2.5 \cdot 10^{-7}$ M (*Lc*TS), M=moles of protein dimers/litre. The fitting curves were obtained with $K_1 = 1 \times 10^7$ M and $K_2 = 6 \times 10^4$ M for *Lc*TS and $K_1 = 9 \times 10^5$ M and $K_2 = 1 \times 10^5$ M for *Ec*TS. Estimated errors are 25 % on K_1s and 50 % on K_2s. T=25 ± 1 °C.

of the W indoles of the protein [23]. Based on the W-DTy r_0 value estimated above in the W-$(P)_n$-DTy compound series, this corresponds to ca. 12 Å. In the *Ec*(*Lc*)TS-DDT structures sketched in Figs. 3 and 4, all the W–DDT (nephthalene ring) distances are larger than 12 Å except for W80 and W83 of *Ec*TS and W82 and W85 for *Lc*TS. Additionally, as shown in Fig. 4D and 4E, the planes of the tryptophan indoles of W83 of *Ec*TS and W82 of *Lc*TS and of the DDT naphthalene in the corresponding structure of the complex are quite far from parallel, suggesting, in case of limited torsional freedom, unfavourable orientation factors for these two excitation-energy transfer donor–acceptor pairs. So, even taking into account the effect of a second DDT molecules symmetrically bound to the other TS monomer, we expect full quenching by DDT only of the emissions from W80 of *Ec*TS and W85 of *Lc*TS. The observed uncomplete quenching of *Lc*TS and *Ec*TS W emissions by DDT is thus consistent with the binding sites found in the *Ec*TS/DDT crystal and in the *Lc*TS/DDT binding model. The fitting procedure was applied to three *Lc*TS and two *Ec*TS data sets. The averages of the best-fit $K_{1,2}$ values are collected in Table 2. They will be commented below together with the results of the calorimetric experiments.

2.3. Thermodynamic signatures of Ec(Lc)TS/DDT binding from isothermal titration calorimetry

Isothermal titration calorimetry (ITC) experiments provided thermodynamic signatures for the *Ec*(*Lc*)TS/DDT binding events. Fig. 7 reports the micro-ITC thermograms for the titrations of a buffered solution of DDT into *Ec*TS and into *Lc*TS, respectively, together with the corresponding plots of the cumulative net heat of binding per mole of protein dimer versus the total ligand-to-protein molar ratio r ($r = [L]_{tot}/[P]_{tot}$) [24,25]. Application of simple thermodynamic models based on one or two equivalent binding sites per dimer did not enable us to adequately fit the two cumulative heat plots. Instead, satisfactory fittings were obtained for both proteins with the same model used to fit the fluorometric results, i.e., a sequential binding model that can be sketched as follows:

Being TS a homodimer, this assumes an initial free protein state P with two equivalent sites, one per monomer, binding DDT with 1:1 stoichiometry. K_1 and K_2 are the stepwise binding constants, whereas $\Delta_b H_1^o$ and $\Delta_b H_2^o$ are the corresponding binding enthalpies expressed per mole of protein dimer [26]. Details of the calorimetric data analysis are provided in the Materials and Methods and in the Supplementary Material. The relevant thermodynamic parameters obtained are reported in Fig. 7 and Table 2.

As regards the higher-affinity binding (subscript 1), we observe a difference in terms of entropic contibution between *Ec*TS and *Lc*TS, 18.8 *vs* 24.4 kJ mol^{-1}, respectively. Although small, this difference may reflect a different scenario in terms of order/disorder changes for this molecular event in the two proteins. Concerning instead lower-affinity DDT binding to the two proteins (subscript 2), relevant differences have emerged indicating that while binding to *Ec*TS is mostly entropically driven, binding to *Lc*TS features the largest enthalpy change among the four binding events and, by far, the smallest change in standard entropy.

3. Discussion

The fluorometric and calorimetric titrations are based on intrinsically different observables, respectively the tryptophan emission efficiency, determined by the protein molecular structure and modulated by proximity of the indole side chains to DDT molecules, and the exchanged heat upon binding reporting on changes in the thermodynamic state functions of the macroscopic protein-DDT-buffer system. Despite the difference in the observables, the two sets of data are remarkably consistent with each other. Quantitative analysis of both of them

Table 2
Ec(*Lc*)TS/DDT $K_{1,2}$ binding constants, corresponding standard free energies, standard binding enthalpies and computed entropic terms obtained from steady-state fluorescence quenching results (Fig. 6 and eqs. 1–5 in the main text and A1 in the Appendix) and from the ITC results (Fig. 7). T=25 ± 1 °C. All thermodynamic function changes are given in kJ/mol. Estimated errors are 10 % on ITC Ks, 5 % on ΔH°s and, respectively, 25 % and 50 % on fluorometrically obtained K_1s and K_2s.

protein	$K_1/10^7$ M^{-1}		ΔH_1°	$T\cdot\Delta S_1^\circ$	$-\Delta G_1^\circ$		$K_2/10^5$ M^{-1}		ΔH_2°	$T\cdot\Delta S_2^\circ$	$-\Delta G_2^\circ$	
	fluo	ITC			fluo	ITC	fluo	ITC			fluo	ITC
***Ec*TS**	0.1	0.19	−17.0	18.8	34.2	35.8	0.8	1.2	−3.8	25.2	28.0	29.0
***Lc*TS**	1	1.2	−16.0	24.4	40.0	40.4	1	2.4	−25.7	5.0	28.5	30.7

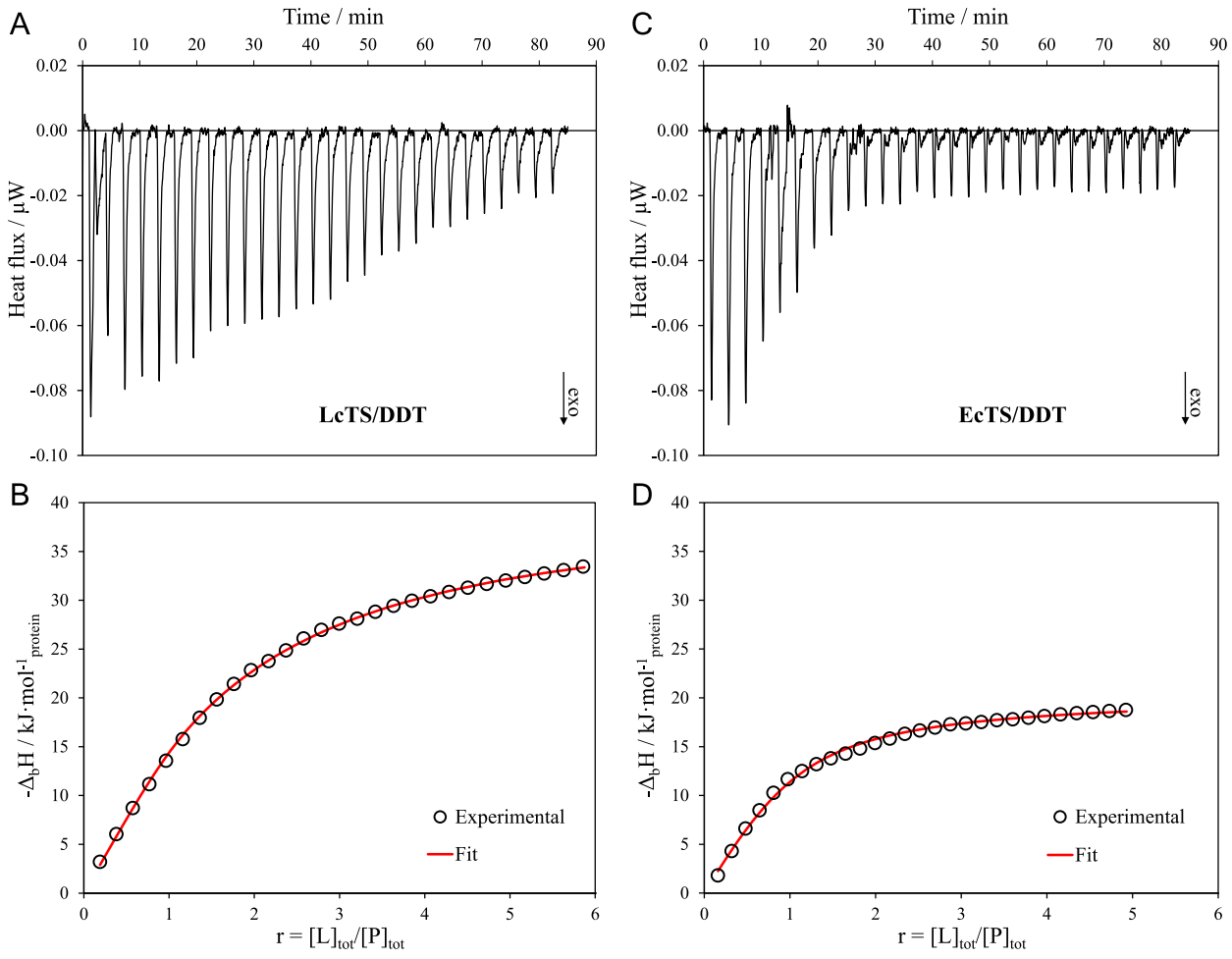

Fig. 7. Calorimetric titration of 0.068 mM DDT into 2.5 µM *Lc*TS (A-B) and of 0.08 mM DDT into 3.5 µM *Ec*TS (C-D). All solutions were prepared in 20 mM potassium phosphate buffer + 30 mM NaCl. pH=6.8; T=25 °C. The upper panels show the raw thermograms after baseline correction; in the lower panels, the cumulative enthalpy (sum of the areas integrated from the upper panel after the correction of the ligand dilution effects), expressed per mole of protein dimer, are plotted versus the total ligand-to-protein molar ratio. The fitting curves (red lines) were obtained according to a two sites sequential binding model. (For interpretation of the references to color in this figure legend, the reader is referred to the web version of this article.)

required adoption of a two-binding-site model for DDT to each protein dimer. The $-\Delta G^{\circ}$/kJ mol^{-1} values obtained from, respectively, the fluorescence and calorimetric data for DDT binding to the higher-affinity sites are very similar, 34.2 *vs* 35.8 kJ mol^{-1} for *Ec*TS and 40 *vs* 40.4 kJ mol^{-1} for *Lc*TS (Table 2). For the lower-affinity binding, the $-\Delta G^{\circ}$/kJ mol^{-1} are, again, almost coincident for *Ec*TS, 28.5 *vs* 29.0, and only slightly different for *Lc*TS, 26.8 *vs* 30.7.

Overall, our most relevant thermodynamic results are: i) a marked drop in affinity between the first and the second binding events, i.e., a negative cooperativity between them. The value of $\Delta\Delta G^{\circ}$ holds 5.7 (fluo) and 6.8 (ITC) kJ mol^{-1} for *Ec*TS, and 13.2 (fluo) and 9.7 (ITC) kJ mol^{-1} for *Lc*TS; ii) affinities of the first binding of DDT to both proteins characterized by entropic terms larger than the enthalpic ones; iii) pronounced enthalpy/entropy compensations between the lower-affinity and the higher-affinity bindings of DDT to each protein (results in rows in Table 2) and, iv) between the lower-affinity bindings to the two proteins (ΔH° and ΔS° columns on the right side of Table 2).

Because, at least for the *Ec*TS:DDT:dUMP complex, X-ray crystallography shows two equal structures for the two monomers, each bound to one dUMP and one DDT molecules, the dissymmetry represented by the observed anti-cooperativity between the two DDT binding events implies that the first binding steals part of its ΔG° from a change in the protein structure that it induces in the second binding site, i.e., across the inter-monomer surface. This portion of standard free energy change is no more available for the second binding event.

Focussing now on a comparison between the first, higher affinity binding of DDT to the two proteins, we found a slightly lower affinity with *Ec*TS than *Lc*TS, $-\Delta G^{\circ}$= 34/36 *vs* 40 kJ mol^{-1}. This 4–6 kJ mol^{-1} difference is mainly ascribable to entropic effects, $\Delta(T\Delta S^{\circ})$ = 5.6 kJ mol^{-1} in favour of *Lc*TS, which may find a structure-related reason. According to the above reported crystallographic evidence, the DDT binding site in an *Ec*TS monomer is smaller than in *Lc*TS, and in the *Ec*TS:DDT:dUMP complex DDT takes a folded structure that, also thanks to several rearrangements in the protein conformation, perfectly fits the enzyme active site and is stabilized by an intramolecular π-π interaction between the distal *N*-dansyl and the ligand tyrosine rings. On the other hand, according to the mentioned computer simulations [6,7], a more extended and relaxed conformation is likely assumed by DDT when binding to the larger active site(s) of *Lc*TS. Another major difference between the X-ray structure of the *Ec*TS ternary complex and the model resulting from the computational analysis of the *Lc*TS ternary complex has been identified in the roles played by Thr78 of the former, able to establish a H bond with the tyrosine O-atom of DDT, and the corresponding residue, His80, of the latter that forms a hydrophobic interaction with the DDT tyrosine ring. Both these differences in the arrangement of the ligand, with a more significant entropy loss associated to ligand folding in the *Ec*TS active site, and in its interactions with Thr78 of *Ec*TS (H bonding) and His80 of *Lc*TS (hydrophobic) are

consistent with the lower entropy change found for the higher-affinity binding to *Ec*TS ($T\Delta S^\circ = 18.8$ kJ mol^{-1}) with respect to *Lc*TS ($T\Delta S^\circ = 24.4$ kJ mol^{-1}).

The lower-affinity DDT binding event exhibits a marked difference in the thermodynamic signature between *Ec*TS and *Lc*TS. The close similarity of the $-\Delta G^\circ$ values at 25 °C results from a remarkable enthalpy/entropy compensation. In fact, relative to the first binding event, the second one features a loss of binding enthalpy, from −17.0 to −3.8 kJ mol^{-1}, and an increased entropic term, from 18.8 to 25.2 kJ mol^{-1}, for *Ec*TS, and a pronounced drop of the entropic term, from 24.4 to 5.0 kJ mol^{-1} and an increased binding enthalpy, from 16.0 to 25.7 for kJ mol^{-1}, for *Lc*TS.

What becomes clear by comparing the X-ray structures of ternary complexes involving a ligand, dUMP and TS, is that a marked local rearrangement of active-site residues takes place upon DDT binding to give the *Ec*TS:DDT:dUMP complex as shown in Fig. 4. Consistently with a representation of these proteins as highly flexible assemblies, we had to invoke the occurrence of longer-range rearrangements to account for the observed anti-cooperativity between the two binding events to each of the two protein dimers. However, following the first DDT binding, communication between the two active sites, i.e., across the inter-monomer surface, induces structural changes that result in a markedly decreased binding enthalpy and an increased entropic gain for the second DDT binding to *Ec*TS, an increased binding enthalpy and a decreased gain in binding entropy for the second binding to *Lc*TS. Because the available structural evidence only concerns an *Ec*TS:DDT:dUMP ternary complex with both binding sites occupied with equal structures, it can hardly serve to produce a molecular-scale structural interpretation of the diverging effects in the two proteins of the first DDT binding on the thermodynamics of the second one.

4. Conclusions

The results of this study provide new insights into the structural bases and the thermodynamic signature of intersite communication in bacterial thymidylate synthases. They suggest that the two active sites in each dimer of the *Lc*TS and *Ec*TS enzymes are not independent of each other, not only when substrate binding occurs, but also when binding of a substrate-unrelated inhibitor such as DDT are concerned. The affinities, stoichiometry, enthalpy and entropy changes of the two bindings of DDT to each dimer of the *Ec*TS and *Lc*TS enzymes were determined by both fluorometric (binding constants and ΔG°s) and calorimetric (full termodynamic signature) titrations. With both enzymes, we observed a marked drop in affinity between the first and second binding events, indicating anticooperativity between the two subsequent binding events in the same enzyme dimer reasonably mediated by long-range perturbations of the protein conformation in one active site induced by DDT binding in the other one. The different conformations assumed by the DDT molecule when it binds to *Lc*TS and *Ec*TS, together with the different types of interactions with amino acid residues in the active site of the two complexes, can explain the difference found in standard binding free energies, that is essentially entropic in nature, for the first, high-affinity DDT binding to the two enzymes. On the other hand, because the crystal structure the *Ec*TS:DDT:dUMP complex features a symmetric dimer with two equal monomers, each bound to one dUMP and one DDT molecules, no structural evidence can help rationalize the peculiar thermodynamic features found for the binding of the second DDT molecule to both proteins. The drop in affinity between the first and the second DDT bindings go together with pronounced entalpy-entropy compensations. The latter, however, take opposite directions with the two enzymes. Overall, the observations clearly indicate that the two TS binding sites are subjected to long-range effects. A similar long-range intersite communication must be responsible for the half-site activity of the *Pneumocystis carinii* model: binding to the second TS active site is hindered or made less favorable following the occupation of the first binding site.

In this context, we see the possibility of new strategies for the design of specific inhibitors of TS enzymes. Developing new high affinity inhibitors able to induce long-range structural rearrangements associated with a decrease in the affinities of the substrates for the second active site, may allow to reduce the inhibitor amount inhibit the enzyme activity, reduce dose and toxicity. This negative cooperativity might be seen as a different manifestation of the half-the-site activity of the TS enzymes: occupation of only one active site would inhibit the protein to a large extent. On the other hand, one might aim at identifying inhibitors able to bind with high affinity to both active sites even in those cases of TSs from infectious microorganisms in which, because of long-range effects, the first binding changes the affinity for the second binding site. The consequence is the potential use of two inhibitors with different structural features showing a preferred affinity for each of the protein active sites. Drug combinations targeting the same dimeric enzyme with sequential binding to the two active sites may represent a useful therapeutic approach. The results of this study provide a basis for further research of the structural and thermodynamic features of intersite communication in thymidylate synthases, including the human one. Moreover it can be a useful example to extend the active −site inhibition enzyme concept to a deeper structure-based inhibition mechanism.

5. Materials and Methods

5.1. Purification of the enzymes and determination of their concentrations

Plasmids that express *L. Casei* TS in the thy *E. Coli* strain x2913 have been previously described [19] The enzyme was purified by column chromatography using phosphocellulose (P11, Biorad) and hydroxyapatite (HAP, Biorad) resin, using phosphate buffer as the eluent. The purified enzymes were stored at −80 °C in 10 mM buffer pH 6.8 and 0.1 mM EDTA. Enzyme activity was determined spectrophotometrically by steady-state kinetic analysis, following the increasing absorbance at 340 nm due to the oxidation reaction of N5,N10-methylenetetraydrofolate to dihydrofolate. 1 mL of reaction solution was formed by standard assay buffer pH 7.4, dUMP (120 microM), 6(R,S)-1-CH2CH4-folate (140 μM), enzyme (0.07 μM). Assays were performed at 20 °C in the standard assay buffer formed by TES (50 mM) at pH7.4, MgCl2 (25 mM), formaldehyde (6.5 mM), EDTA (1 mM), and 2-mercaptoethanol (75 mM).

The concentrations of the proteins were determined spectrophotometrically at 280 nm using molar extinction coefficients for the dimers $\varepsilon(280) = 103000$ M^{-1}cm^{-1} and $\varepsilon(280) = 117600$ M^{-1}cm^{-1} for *Ec*TS and *Lc*TS, respectively. These were determined from the numbers of tyrosines (n_Y) and tryptophans (n_W) in the 1JG0 and 1LCA PDB sequences (respectively, n_Y=18, n_W=14 and n_Y=28, n_W=14) and the usual contributions of tyrosine (1450 M^{-1}cm^{-1}) and tryptophan (5500 M^{-1} cm^{-1}) to the $\varepsilon(280)$ of a protein.

5.2. Isothermal titration calorimetry

ITC titrations were performed at 25 °C by using a VP-ITC MicroCalorimeter (MicroCal, Inc.) having an active cell volume of 1.440 mL and equipped with a 10 μL injection syringe. All experiments were carried out in 20 mM potassium phosphate buffer + 30 mM NaCl at pH 6.8 by injecting 10 μL aliquots of a solution of DDT (ligand) into the protein solution previously saturated with deoxyuridine monophosphate (1:60), and the concentrations used were 0.08 mM DDT into 3.5 μM EcTS and 0.068 mM DDT into 2.5 μM LcTS. All the solutions were degassed before use. The reaction mixture in the sample cell was stirred during the titration.

5.3. The enzyme activity was also checked after sample concentration

The thermal effect related to each injection was corrected by subtracting the heat related to the ligand dilution effects into the buffer to obtain the net heat per injection. Thermodynamic binding models were

tested to interpret the ITC data [25].

Briefly, the observable enthalpy is given by

$$\Delta H(T,p,\mu_L) = -R\left[\frac{\partial \ln Q}{\partial(1/T)}\right]_{p,\mu_L} \quad (6)$$

and the degree of association, that is the concentration ratio $\overline{x}$ = [bound ligand]/[total protein], is given by

$$\overline{x} = RT\left[\frac{\partial \ln Q}{\partial \mu_L}\right]_{T,P} = \left[\frac{\partial \ln Q}{\partial \ln[L]}\right]_{T,P} \quad (7)$$

where R is the universal gas constant, μL is the chemical potential of the free ligand, [L] is the concentration of the free ligand, and Q is the partition function of the system referred to the free protein state [26]. Since we can approximate these systems as diluted solutions, the thermodynamic activities of the solutes may be replaced with their molar concentrations. Under this assumption, the partition function is the sum

$$Q = \sum_{j=0}^{n} [P_j]/[P_0] \quad (8)$$

of the concentrations of all protein species, P_j, referred to the free protein, P_0. Q depends on the assumptions made on the association (binding) mechanism and is the key function used to simulate the enthalpy so as to check the model with the experimental data and to obtain the association (or binding) constant, K_b, and the binding enthalpy, ΔH_b°. The binding constant is a dimensionless quantity by definition. However, in order to stress the approximation of the thermodynamic activities with the molar concentrations, the use of M^{-1} units for this parameter is widely used and was adopted in this article.

The fit attempts based on the binding models were accomplished using the nonlinear Levenberg–Marquardt method [27]. The errors of each fitting parameter were calculated with a 95.4 % confidence limit by the Monte Carlo simulation method.

5.4. Absorption and fluorescence

Absorption spectra were measured with a Lambda 15 Perkin-Elmer spectrophotometer. Fluorescence measurements were performed at room temperature (20 ± 1 °C) on a Spex-Jobin Yvon Fluoromax 2 spectrofluorometer. The intensity of the TS W fluorescence at the emission maximum was monitored following addition of DDT to *Ec*(*Lc*) TS pre-saturated with 100 μM dUMP. The protein concentration was corrected for the volume change, of the order of 10 % at titration end. Quantitative analysis of results was done as described in the Results and in the Supplementary Material.

5.5. Synthesis of polyprolines

Dansylchloride, protected amino acids (FMOC-tyrosine, FMOC-tryptophan and FMOC-Proline), coupling activators (HOBt, PyBop and DIPEA), pyridine and solvents were purchased from Aldrich, Sigma, Fluka and Novabiochem. Progress of the reactions was monitored by TLC on silica gel plates. 1H NMR spectra were recorded on Bruker DPX200 and Bruker AMX400. Mass spectrometry analyses were performed using the Agilent 6540 quadrupole time of flight (Q-TOF) mass analyser. Products purification was performed using AKTAprime instrument. UV–visible absorption spectra were recorded using Cary 50 spectrophotometer, while fluorescence spectra were recorded using the Cary 100. Polyproline peptides were synthesized using a Büchi Syncore synthesizer using Rink-amide resin according to Fmoc (9-fluorenylmethoxycarbonyl) methodology. All peptides of defined length (containing 3, 6, 9 and 12 Pro residues) were synthesized using as carboxyl-terminal aminoacid O-danyl-tyrosine. The Rink Amide resin (4-(2′,4′-dimethoxyphenyl-Fmoc-aminomethyl)-phenoxy resin) was employed with a loading of 0.56 mmol/g active site, it was calculated using the monitoring of Fmoc removal by UV spectrophotometry (λ = 290 nm). The Fmoc deprotection was accomplished with a solution of piperidine in DMF (20 %). Peptide couplings were activated by the addiction at the solution of the appropriate Fmoc-protected aminoacid in DMF with 3 eq. of 1-hydroxybenzotriazole (HOBt), 3 eq. of Benzotriazol-1-yl-oxytripyrrolidinophosphonium hexafluorophosphate (PyBOP) and 5 eq. of N,N‘-Diisopropylethylamine (DIEA). The mixture was stirring for 3 h, then the completeness of coupling was carefully monitored by Kaiser test and chloranil test respective for tryphtophan and dansyltyrosine and for proline. Upon completion of chain assembly, the Fmoc group was removed as above. The peptide was cleaved from the solid support using Reagent K (TFA: H_2O: thioanisole: ethanedithiol; phenol 82:5:5:3:5), two washing of 1 h (4 mL); the mixture was filtered and the resultant solution was precipitate with cold diethyl ether (Et_2O) and washed with cold Et_2O. The peptides was then purified using a semipreparative C18 reverse-phase column (Sephadex C-18 applied at the purification system AKTA prime) by applying a gradient from 10 % to 50 % acetonitrile in 0.1 % TFA/water. Fractions contained the pure petide (as confirmed by electrospray ionization mass spectroscopy) were lyophilizated. Q-TOF HRMS Exact mass: Calcd. for W-(P)3-DTy:891,3625; found 891.3771, Exact mass Calcd. for W-$(P)_6$-DTy: 1182,5208; found: 1182.5208, Exact mass Calcd. for W-$(P)_9$-DTy: 1473,7430; found: 736,8715, Exact mass W-$(P)_{12}$-DTy: 1764,8374; found: 883,4290.

5.6. Conformational analysis of the W-$(P)_6$-DT peptide

The W-$(P)_6$-DT peptide sequence was designed by the 2D builder implemented in the Maestro suite. Minimization was perfomed within the LigPrep module. Pymol (version 2.5.2) was employed to visualize the conformations and compute the W-DT distances.

CRediT authorship contribution statement

Alberto Venturelli: Writing – review & editing, Writing – original draft, Investigation. **Giambattista Guaitoli:** Writing – review & editing, Writing – original draft, Methodology, Investigation, Conceptualization. **Davide Vanossi:** Methodology. **Francesca Saitta:** Methodology, Investigation. **Dimitrios Fessas:** Writing – review & editing, Writing – original draft, Supervision, Methodology, Investigation, Formal analysis, Conceptualization. **Simone Vitiello:** Methodology, Investigation. **Giulia Malpezzi:** Methodology, Investigation. **Daniele Aiello:** Methodology, Investigation. **Stefania Ferrari:** Methodology, Conceptualization. **Donatella Tondi:** Conceptualization. **Glauco Ponterini:** Writing – review & editing, Writing – original draft, Supervision, Investigation, Formal analysis, Conceptualization. **Maria Paola Costi:** Writing – review & editing, Writing – original draft, Supervision, Methodology, Investigation, Funding acquisition, Conceptualization.

Declaration of competing interest

The authors declare that they have no known competing financial interests or personal relationships that could have appeared to influence the work reported in this paper.

Acknowledgments

The research leading to these results has received funding from AIRC under IG 2021 – ID 25785 – P.I. Costi Maria Paola and by intramural grant University of Modena and Reggio.

Appendix A. Supplementary data

Supplementary data to this article can be found online at https://doi.org/10.1016/j.bioorg.2024.107663.

References

[1] P.M. Wilson, P.V. Danenberg, P.G. Johnston, H.-J. Lenz, R.D. Ladner, Standing the test of time: targeting thymidylate biosynthesis in cancer therapy, Nat. Rev. Clin. Oncol. 11 (2014) 282–298, https://doi.org/10.1038/nrclinonc.2014.51.

[2] R. Luciani, P. Saxena, S. Surade, M. Santucci, A. Venturelli, C. Borsari, G. Marverti, G. Ponterini, S. Ferrari, T.L. Blundell, M.P. Costi, Virtual Screening and X-ray Crystallography Identify Non-Substrate Analog Inhibitors of Flavin-Dependent Thymidylate Synthase, J. Med. Chem. 59 (2016) 9269–9275, https://doi.org/10.1021/acs.jmedchem.6b00977.

[3] J. Bré, A.L. Dickson, O.J. Read, Y. Zhang, F.G. McKissock, P. Mullen, P. Tang, G. M. Zickuhr, C.M. Czekster, D.J. Harrison, The novel anti-cancer fluoropyrimidine NUC-3373 is a potent inhibitor of thymidylate synthase and an effective DNA-damaging agent, Cancer Chemother. Pharmacol. 91 (2023) 401–412, https://doi.org/10.1007/s00280-023-04528-5.

[4] P.M. Costi, M. Rinaldi, D. Tondi, P. Pecorari, D. Barlocco, S. Ghelli, R.M. Stroud, D. V. Santi, T.J. Stout, C. Musiu, E.M. Marangiu, A. Pani, D. Congiu, G.A. Loi, P. La Colla, Phthalein derivatives as a new tool for selectivity in thymidylate synthase inhibition, J. Med. Chem. 42 (1999) 2112–2124, https://doi.org/10.1021/jm9900016.

[5] M.P. Costi, A. Gelain, D. Barlocco, S. Ghelli, F. Soragni, F. Reniero, T. Rossi, A. Ruberto, C. Guillou, A. Cavazzuti, C. Casolari, S. Ferrari, Antibacterial agent discovery using thymidylate synthase biolibrary screening, J. Med. Chem. 49 (2006) 5958–5968, https://doi.org/10.1021/jm051187d.

[6] S. Mangani, L. Cancian, R. Leone, C. Pozzi, S. Lazzari, R. Luciani, S. Ferrari, M. P. Costi, `Identification of the binding modes of N-phenylphthalimides inhibiting bacterial thymidylate synthase through X-ray crystallography screening, J. Med. Chem. 54 (2011) 5454–5467, https://doi.org/10.1021/jm2005018.

[7] D. Tondi, U. Slomczynska, M.P. Costi, D.M. Watterson, S. Ghelli, B.K. Shoichet, Structure-based discovery and in-parallel optimization of novelcompetitive inhibitors of thymidylate synthase, Chem. Biol. 6 (1999) 319–331, https://doi.org/10.1016/S1074-5521(99)80077-5.

[8] T.A. Fritz, D. Tondi, J.S. Finer-Moore, M.P. Costi, R.M. Stroud, Predicting and harnessing protein flexibility in the design of species-specific inhibitors of thymidylate synthase1,21Escherichia coli thymidylate synthase numbering is used unless otherwise noted.2PDB coordinates have been deposited with the RCSB with ac, Chem. Biol. 8 (2001) 981–995, https://doi.org/10.1016/S1074-5521(01)00067-9.

[9] T. Dasgupta, K.S. Anderson, Probing the role of parasite-specific, distant structural regions on communication and catalysis in the bifunctional thymidylate synthase−dihydrofolate reductase from *Plasmodium falciparum*, Biochemistry. 47 (2008) 1336–1345, https://doi.org/10.1021/bi701624u.

[10] E.M. Koehn, T. Fleischmann, J.A. Conrad, B.A. Palfey, S.A. Lesley, I.I. Mathews, A. Kohen, An unusual mechanism of thymidylate biosynthesis in organisms containing the thyX gene, Nature. 458 (2009) 919–923, https://doi.org/10.1038/nature07973.

[11] A.C. Muscroft-Taylor, T.P. Soares da Costa, J.A. Gerrard, New insights into the mechanism of dihydrodipicolinate synthase using isothermal titration calorimetry, Biochimie. 92 (2010) 254–262, https://doi.org/10.1016/j.biochi.2009.12.004.

[12] P.J. Sapienza, B.T. Falk, A.L. Lee, Bacterial thymidylate synthase binds two molecules of substrate and cofactor without cooperativity, J. Am. Chem. Soc. 137 (2015) 14260–14263, https://doi.org/10.1021/jacs.5b10128.

[13] J.P. Bonin, P.J. Sapienza, E. Wilkerson, D. Goldfarb, L. Wang, L. Herring, X. Chen, M.B. Major, A.L. Lee, Positive cooperativity in substrate binding by human thymidylate synthase, Biophys. J. 117 (2019) 1074–1084, https://doi.org/10.1016/j.bpj.2019.08.015.

[14] L.L. Lovelace, L.M. Gibson, Lebioda, Cooperative inhibition of human thymidylate synthase by mixtures of active site binding and allosteric inhibitors, Biochemistry. 46 (2007) 2823–2830, https://doi.org/10.1021/bi061309j.

[15] E.F. Johnson, W. Hinz, C.E. Atreya, F. Maley, K.S. Anderson, Mechanistic characterization of Toxoplasma gondii thymidylate synthase (TS-DHFR)-dihydrofolate reductase, J. Biol. Chem. 277 (2002) 43126–43136, https://doi.org/10.1074/jbc.M206523200.

[16] A.L. Lee, P.J. Sapienza, Thermodynamic and NMR assessment of ligand cooperativity and intersubunit communication in symmetric dimers: application to thymidylate synthase, Front. Mol. Biosci. 5 (2018), https://doi.org/10.3389/fmolb.2018.00047.

[17] A.C. Anderson, R.H. O'Neil, W.L. DeLano, R.M. Stroud, The structural mechanism for half-the-sites reactivity in an enzyme, thymidylate synthase, involves a relay of changes between subunits, Biochemistry. 38 (1999) 13829–13836, https://doi.org/10.1021/bi991610i.

[18] L. Costantino, S. Ferrari, M. Santucci, O.M.H. Salo-Ahen, E. Carosati, S. Franchini, A. Lauriola, C. Pozzi, M. Trande, G. Gozzi, P. Saxena, G. Cannazza, L. Losi, D. Cardinale, A. Venturelli, A. Quotadamo, P. Linciano, L. Tagliazucchi, M. G. Moschella, R. Guerrini, S. Pacifico, R. Luciani, F. Genovese, S. Henrich, S. Alboni, N. Santarem, A. da S. Cordeiro, E. Giovannetti, G.J. Peters, P. Pinton, A. Rimessi, G. Cruciani, R.M. Stroud, R.C. Wade, S. Mangani, G. Marverti, D. D'arca, G. Ponterini, M.P. Costi, Destabilizers of the thymidylate synthase homodimer accelerate its proteasomal degradation and inhibit cancer growth, Elife. 11 (2022), https://doi.org/10.7554/ELIFE.73862.

[19] M.P. Costi, D. Tondi, M. Rinaldi, D. Barlocco, P. Pecorari, F. Soragni, A. Venturelli, R.M. Stroud, Structure-based studies on species-specific inhibition of thymidylate synthase, Biochim. Biophys. Acta - Mol. Basis Dis. 1587 (2002) 206–214, https://doi.org/10.1016/S0925-4439(02)00083-2.

[20] J. Finer-Moore, E.B. Fauman, P.G. Foster, K.M. Perry, D.V. Santi, R.M. Stroud, Refined structures of substrate-bound and phosphate-bound thymidylate synthase from Lactobacillus casei, J. Mol. Biol. 232 (1993) 1101–1116, https://doi.org/10.1006/jmbi.1993.1463.

[21] B. Schuler, E.A. Lipman, P.J. Steinbach, M. Kumke, W.A. Eaton, Polyproline and the "spectroscopic ruler" revisited with single-molecule fluorescence, Proc. Natl. Acad. Sci. 102 (2005) 2754–2759, https://doi.org/10.1073/pnas.0408164102.

[22] T. Edsall, H. Gutfreund, Biothermodynamics. John Wiley and Sons, 1984, Chapt.5. n.d.

[23] B. Valeur M.N. Berberan-Santos Molecular fluorescence: principles and applications 2nd Ed., 2012 Wiley-VCH Verlag 10.1002/9783527650002 Ch. 8.

[24] K. Tripsianes, T. Madl, M. Machyna, D. Fessas, C. Englbrecht, U. Fischer, K. M. Neugebauer, M. Sattler, Structural basis for dimethylarginine recognition by the Tudor domains of human SMN and SPF30 proteins, Nat. Struct. Mol. Biol. 18 (2011) 1414–1420, https://doi.org/10.1038/nsmb.2185.

[25] S. Capaldi, G. Saccomani, D. Fessas, M. Signorelli, M. Perduca, H.L. Monaco, The X-ray structure of zebrafish (*Danio rerio*) ileal bile acid-binding protein reveals the presence of binding sites on the surface of the protein molecule, J. Mol. Biol. 385 (2009) 99–116, https://doi.org/10.1016/j.jmb.2008.10.007.

[26] J.& G.S.J. Wyman, Binding and Linkage: Functional chemistry of biological macromolecules by Jeffries Wyman and Stanley J. Gil, 1990.

[27] W.H. Press, S.A. Teukolsky, W.T. Vetterling, B.P. Flannery, Numerical Recipes, The Art of Scientific Computing, Cambridge, UK, 1989.